ACS OMEGA

http://pubs.acs.org/journal/acsodf

Article

Characterization of Hen's Egg White To Use It as a Novel Platform To Culture Three-Dimensional Multicellular Tumor Spheroids

Perumalsamy Balaji, Anbazhagan Murugadas, Arunachalam Ramkumar, Ramasamy Thirumurugan, Sellathamby Shanmugaapriya, and Mohammad Abdulkader Akbarsha*

Cite This: https://dx.doi.org/10.1021/acsomega.0c02508

Read Online

ACCESS | Metrics & More | Article Recommendations

ABSTRACT: We are standardizing protocols to develop egg white (EW) as a cost-effective platform for culture of three-dimensional (3-D) multicellular tumor spheroids for application in understanding tumor microenvironments and drug screening. In this article, we describe several physical and physiological characteristics of EW to use it as 3-D cell culture platform. Field emission scanning electron microscopy revealed the presence of different microstructures. Hydrodynamic size distribution data indicated nano- and micron-sized particles. Rheological measurements revealed the viscosity and viscoelastic behavior appropriate for maintaining cell viability and supporting 3-D cell growth under high-sheer conditions. It was found that thereis no autofluorescence, a requirement for imparting transparency and for microscopic observations of the spheroids. The EW facilitated the development of 3-D tumor spheroids, with an emphasis of difference in cell proliferation and intercellular cytoskeletal organization between two-dimensional and 3-D spheroid cultures. Put together, EW proves to be a cost-affordable and simple platform for 3-D culture of tumor spheroids.

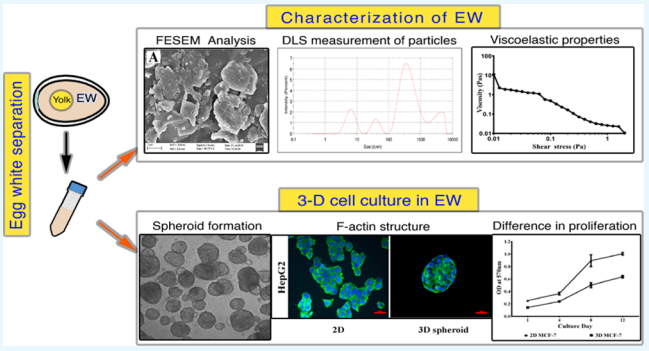

1. INTRODUCTION

Two-dimensional (2-D) cell culture is an important technique practiced in cancer biology research to understand the molecular mechanisms of tumor development and invasion and to find appropriate drug targets. Even though it has been in extensive use during the past several decades, certain limitations have affected its use as an effective investigative tool in cancer biology. Importantly, 2-D culture does not always ensure productivity, whereupon cost and failure rates increase.[1] Going a little deep into the issue, cells cultured in the 2-D format on a rigid substrate are deficient in cell−cell and cell−extracellular matrix (ECM) communications causing stretched cytoskeletal elements. This in turn affects the cellular polarity and leads to aberrant gene and protein expressions.[1−4] To overcome these limitations, models resulting from three-dimensional (3-D) cultures have come up. In 3-D culture systems, cells are cultured by embedding in a complex 3-D native ECM-like substrate providing cell−cell as well as cell−ECM communications, which help in maintaining the intercellular junctional complexes and cell polarity. This facilitates the cells to simulate the functional and physiological characteristics of in vivo tumors.[5,6] Especially, the 3-D multicellular tumor spheroid (MTS) models facilitate a better understanding of tumor growth, invasiveness, tumor cell architecture, cell-signaling mechanisms, tumor cell dormancy, angiogenesis, and so forth than other 3-D models.[7,8] Importantly, properties of solid tumors, such as spatial organization of cells, expression of genes, different zones of proliferation, and involvement of local microenvironments with the disease, can be recaptured by culturing cells in 3-D MTS.[9−11]

Use of a hydrogel/scaffold is an attractive approach to culture cells in the 3-D MTS format as it provides mechanical as well as structural supports to the cells in a way similar to the native tissue. The microstructures and interconnected pores present in hydrogels/scaffolds enable retention of water and efficient transport of nutrients and wastes.[12] Our study aims at using whole egg white (EW) from hen (*Gallus gallus domesticus*; White Leghorn breed) as an easy-to-prepare and cost-affordable platform as an alternative to hydrogels/scaffolds to produce 3-D MTS. The composition of EW has already been adequately characterized. It is composed of 9.7−10.6% protein by weight, which contributes to the develop-

Received: May 28, 2020
Accepted: July 23, 2020

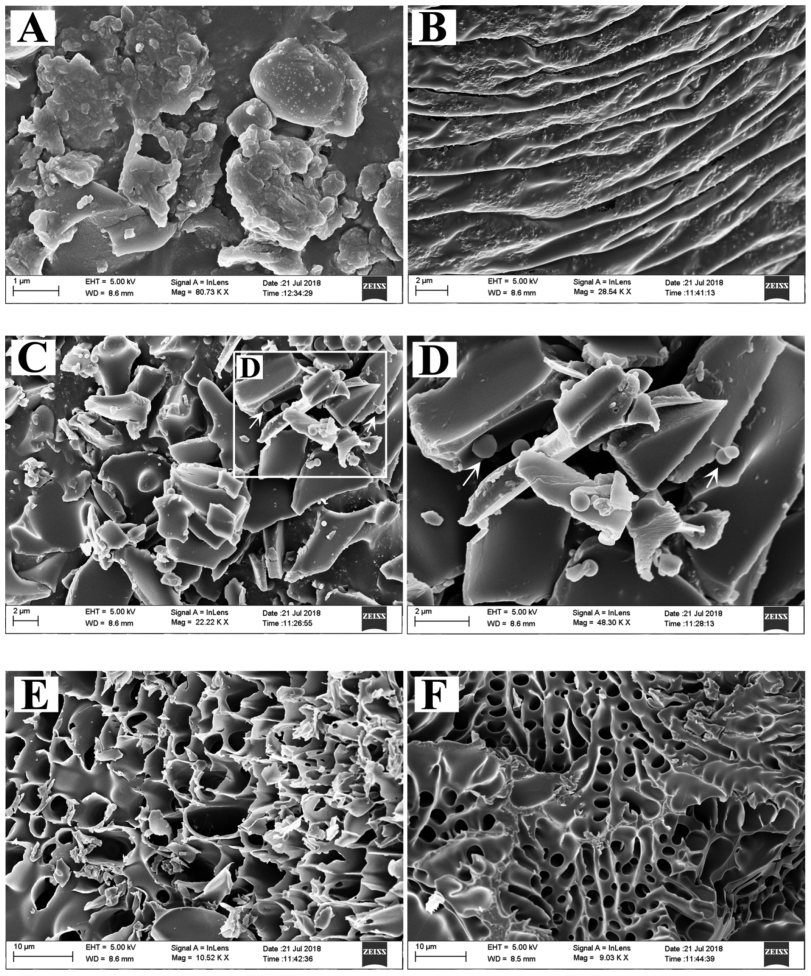

Figure 1. Microstructure of the EW analyzed by SEM. Different morphological features were observed. (A,B) Aggregated and self-assembled morphologies, respectively. Flakes and sphere structures are presented in (C). (D) Inset in (C). (E,F) Two different porous structures observed in EW.

ment of embryo.[13,14] More importantly, extracts and proteins from EW support cell growth and proliferation.[15,16] Therefore, EW can serve as a suitable material to culture cells in the 3-D format. Furthermore, the nontoxic property, biocompatibility, and biodegradability of EW are added advantages to use it as a 3-D cell culture platform.[17−19] We conducted a preliminary study of an EW cryogel bioscaffold for use in 3-D MTS and found advantages such as extensive porosity, homogeneous pore size, and amide linkages during cross-linking, in addition to cost-affordability.[20]

The present study, developing further on our earlier findings, aimed at characterizing the morphological features, particle size distribution, rheological properties, and optical properties of EW toward its application as a convenient platform to culture cells in the 3-D MTS format. The effect of shear stress while handling EW was addressed. The different cell types cultured as 3-D MTS in EW were analyzed adopting light microscopy. The proliferation efficiencies between the 2-D culture and 3-D MTS were compared over the period of incubation. The difference in the structure of the cytoskeleton between the 2-D and 3-D MTS models was analyzed.

2. RESULTS AND DISCUSSION

2.1. Microstructural Characteristics of EW. The surface morphological features of the EW were analyzed using field emission scanning electron microscopy (FESEM) measurements. The results showed that the EW contains different morphologies with different ranges of sizes, nano- to micrometers, among which interconnected aggregated structures were predominant (Figure 1A). Furthermore, self-assembled morphologies (Figure 1B), flakes (Figure 1C), sphere-like structures (Figure 1D), and porous structures of different sizes (Figure 1E,F) were also observed. The spheres measured a diameter between 0.22 and 1.5 μm and the average sphere size was 0.65 μm (Figure 1C). The dimensions of flakes ($L \times W$) were in the range of 1.68 × 1.02 μm to 6.81 × 5.48 μm (Figure 1C,D). Also, the diameters of two different porous structures, shown in Figure 1E,F, were between 2.28 μm and 7.47 μm with an average pore size of 4.5 μm and 0.78 μm × 3.25 μm with an average pore size of 2.33 μm, respectively.

It is well known that hen's EW, a thick fluid, contains 11% proteins. Ovalbumin, conalbumin, ovomucoid, ovotransferrin, and lysozyme are the major proteins. The other constituents are fat 0.2%, ash 0.8%, and water 88%. The different morphologies observed in scanning electron microscopy (SEM) analysis are reflections of the different compositions.[13] Ovalbumin constitutes 54% of total dry mass. EW albumins undergo aggregation at this concentration. Also, it is known that EW albumins can undergo aggregation in the pH range 4−9 at room temperature.[21−23] Moreover, the polar and

https://dx.doi.org/10.1021/acsomega.0c02508
ACS Omega XXXX, XXX, XXX−XXX

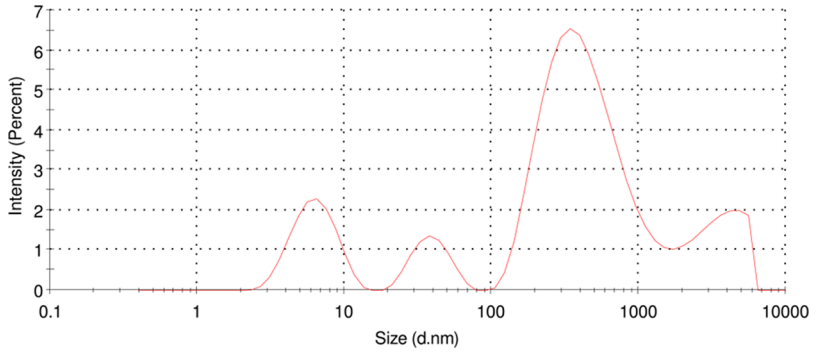

Figure 2. Hydrodynamic size distribution of EW analyzed by DLS measurement.

nonpolar proteins present in EW may be responsible for the different structures formed in EW. Especially, the polar nature of the structural protein ovomucin is thought be the reason for aggregation of EW to filamentous and fibroid structures. To the best of our knowledge, this is the first report of elucidation of the different morphologies present in the raw EW of hen where previous findings reveal only the structure of proteins in their purest form. Furthermore, the hydrodynamic size distribution of the EW was assessed adopting dynamic light scattering (DLS). The average size was found to be 485.7, 3568, and 6.469 nm (Figure 2). The results obtained from the particle size measurement confirm the presence of nano- to micron-sized particles in the EW and substantiate the data obtained from FESEM analysis (Figure 1).

2.2. Rheological Characteristics. ECM is a macromolecular structure that provides mechanical and structural supports to cells in tissues and maintains tissue polarity via the cell−ECM interaction. More precisely, the viscoelasticity of the ECM determines the fate of tissue homeostasis. Therefore, it is necessary to provide in vivo relevant physiological force to the cells in order to maintain their original tissue homeostasis under laboratory conditions. In our study, the measurement of viscosity against the shear stress shows gel-like elastic behavior at the low stress level. At high shear stress, the overall viscosity of EW decreased to near 0.1 Pa s, and a fluid-like behavior was observed (Figure 3).

The study of viscoelasticity in oscillation frequency sweep mode confirms the transition from a gel-like behavior into a fluid-like under the constant strain. The result shows frequency-dependent storage (G') and loss (G'') modules. The storage module (G'), responsible for elastic characteristics, was initially higher than the loss module (G'') at low frequencies ($G' > G''$). It was decreased significantly below the loss module (G'') in response to increased frequencies and, as a result, the viscous behavior prevails over the elastic nature of EW (Figure 4). The result justifies that the elastic behavior

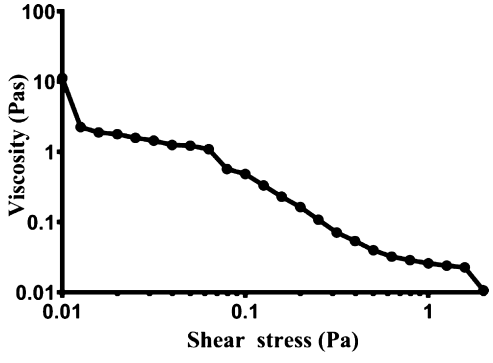

Figure 3. Apparent viscosity measurement in relation to shear stress shows high viscosity at low shear stress, which decreased with increased shear stress.

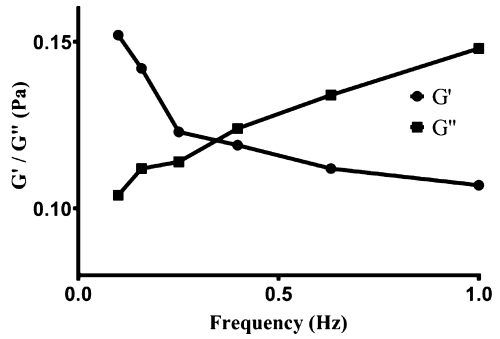

Figure 4. Frequency-dependent storage (G') and loss modules (G'') exhibit a viscous behavior with increased frequencies prevailed over the elastic behavior observed at the rest.

maintained at rest will keep the cells in the viscous state, which is advantageous to culture the cells as spheroids. As seen in SEM analysis, most of the particles in EW that were revealed as macromolecules were aggregates that help to maintain EW in a highly viscous form. Under the deformation or shearing, these macromolecules may disintegrate into smaller particles. At this stage, the material shows shear-thinning flow behavior, which may be useful to transfer the EW using syringes. Because the EW has this property, the cells can get mixed homogeneously with the EW, whereupon syringes and microtips can be used to handle the cell−EW suspension. The viscosity of EW, as found in the experiment, was 11.2 Pa G', which is advantageous for mammalian cell culture applications. Collagen matrices affording $G' \approx 4-60$ Pa are appropriate to culture 3D soft tissue.[24]

Importantly, the resurgence of viscosity after stress was measured by shearing the material at 500 s^{-1} for 30 s. It was observed that the viscosity of EW was established immediately after shearing stopped (Figure 5). However, measurement of dynamic complex viscosity, η^*, versus angular frequency showed a decrease in the structural strength of the EW material after shearing. In this experiment, constant strain was applied to decrease the structural strength of the EW material and to study the equilibrium between internal structural breakdown and rebuilding. The result shows a decrease in η^* under the effect of increasing frequency (before shearing), and

https://dx.doi.org/10.1021/acsomega.0c02508
ACS Omega XXXX, XXX, XXX−XXX

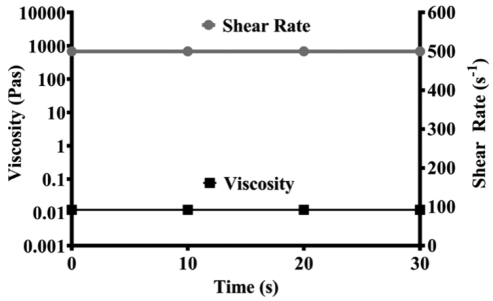

Figure 5. Evaluating the EW viscosity after shearing the gel at 500 s^{-1} for 30 s demonstrates instant recovery of viscosity after shearing stopped.

thereafter, start of structural build up upon deformation is slowed (after shearing) (Figure 6). However, complex viscosity

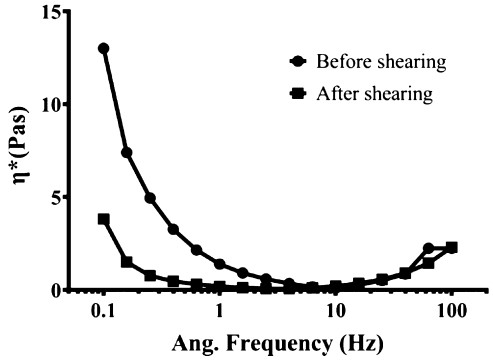

Figure 6. Dynamic complex viscosity, η^*, of EW measured before and after shearing. The results represent the lack of complete recovery of η^*, describing the structural deformation after shearing.

was not fully recovered and the reduction may possibly be due to disruption of the internal network structure present in the EW. This reduction in complex viscosity after shearing may affect the strength of the material while dealing with the EW during experiment and it might affect homogeneous spheroid formation. Overall, the results from the rheological experiments facilitate the conclusion that the EW possesses viscoelastic properties favorable to culture the cells. Especially, transition from an elastic state to a fluid-like state and shear stress viscosity that is 11.2 Pa G' observed in EW are suitable to mimic physiological ECM for culture of soft tissues.[24] On the other hand, the disruption in the internal structure of EW observed under shearing conditions may affect its function as a cell culture platform.

2.3. Injectability of EW for Cell Culture. The effect of sheer stress on viability of cells while handling cell−EW suspension was measured using syringes of different volumes and needles of different gauge sizes. The results from the MTT viability assay indicated that viability of cells was not affected even in the case of smallest needle used (#26) (Figure 7). The fluid-like behavior of EW as inferred from the rheological observation may keep the cells viable even after high shear. It is believed that EW may reduce the volume of suspension under high shear stress, and the high composition of macromolecules present in EW may contribute to this phenomenon. The 1−300 μL pipette tip, routinely used in laboratory experiments, is equivalent to a #20 needle.[25]

2.4. Optical Properties. Visualization of 3-D cultured cells, without disturbing the culture conditions, is an important

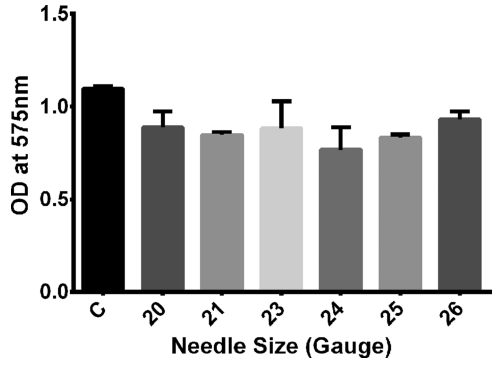

Figure 7. Injectability of EW for cell culture. The results after the MTT assay show that the viability was not affected by injection with syringes with needles of different gauge sizes. Error bars represent mean ± SD (n = 6).

aspect in developing a transparent cell culture medium. It depends greatly on optical properties of the material used in the 3-D culture. In our study, the optical property of EW was analyzed by measuring the absorbance and fluorescence spectra. The results from the UV−visible spectral analysis show that the peak observed at 300 nm corresponds to the high absorbance light (Figure 8A). Therefore, it is concluded that the optical detection near 300 nm may be limited in the EW. However, it is noted that the wavelength of visible light used in most of the optical microscopes ranges from 400 to 700 nm. Thus, the absorbance at 300 nm may not hinder

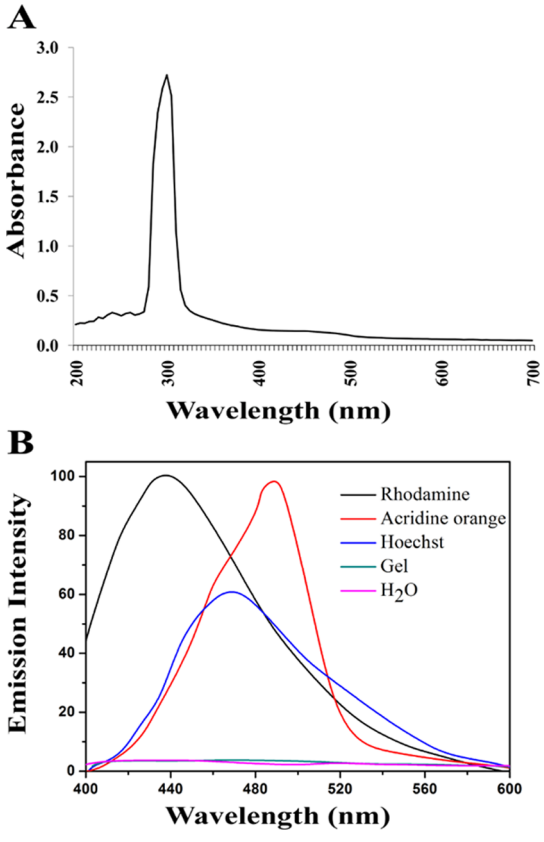

Figure 8. Optical properties of EW. (A) Absorbance spectrum of EW. The peak was recorded at 300 nm, corresponding to the high absorbance at 300 nm. (B) No autofluorescence was recorded in the fluorescence spectral analysis of EW compared to pure water.

https://dx.doi.org/10.1021/acsomega.0c02508
ACS Omega XXXX, XXX, XXX−XXX

visualization in the optical microscope and be helpful in experimenting with live cell imaging. In addition, the property of autofluorescence of EW was measured by scanning the fluorescence spectra after excitation at 350, 480, and 511 nm wherein hoechst 33258, acridine orange, and rhodamine 123 were used as the respective reference dyes. The excitation wavelength chosen in our study is based on a wide range of fluorescent dyes used in biological imaging under this wavelength range. No fluorescent emission was observed on excitation at different wavelengths (Figure 8B). Thus, it is evident that the EW does not fluoresce and, so, suitable for most of the fluorescence-based microscopic observations and fluorescence-related quantitative methods.

2.5. Biocompatibility. The biocompatibility of EW was tested using A549, MCF7, HepG2, and HEK293 cells. During the experiments, different proportions of EW and growth medium were mixed and added to wells of a 96-well culture plate. The total volume was set as 200 μL and EW/culture medium concentrations were maintained at five proportions: 0:200, 50:150, 100:100, 150:50, and 200:0 for groups 1, 2, 3, 4, and 5, respectively. The results from the MTT assay after 48 h of incubation with EW showed that the percentages of viability of all four cell lines were significantly increased at 50 μL and 100 μL EW concentrations compared to the untreated or 0 μL and 200 μL. The rate of viability was observed to be higher at 100 μL EW than the other concentrations (Figure 9). The

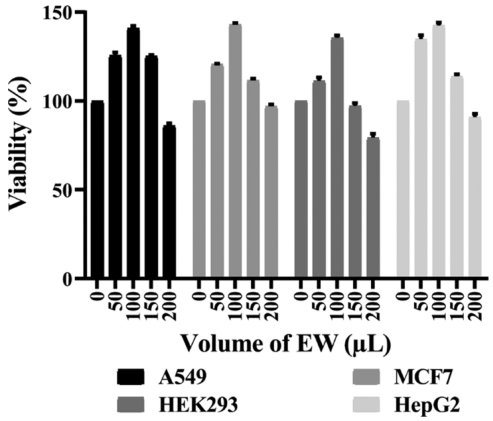

Figure 9. Biocompatibility of EW with A549, MCF7, HepG2, and HEK293 cells adopting the MTT assay. The results show difference in percentage of viability against different volumes of EW and higher viability at 100 μL EW compared to other concentrations. Error bars represent mean ± SD (n = 3).

viability for all four cells was decreased at a volume of 200 μL of EW. The alkaline pH of EW is also a factor that would affect cell viability. The alkaline pH of isolated EW (pH 9−10) was reduced to 7−8 by adding the growth medium when beginning the cell culture. It is believed that while using a low volume of EW, the alkalinity of EW may get neutralized by adding culture media as in groups 2 and 3. However in groups 4 and 5, less or no medium was added, which means less chance of neutralizing the pH. The results reveal that increase of the EW concentration affects the cell viability, and the alkaline pH must be neutralized with growth media for cell culture experiments. Most importantly, the EW contains numerous proteins that promote cell proliferation when the pH gets neutralized.

2.6. Light Microscopic Morphological Features of Spheroids Grown in EW. The cells generally appear polygonal or cuboidal when cultured in a monolayer. However, when cultured as a spheroid, their morphology is cell-line specific.[10,26,27] Four morphological forms have been reported: grape-bunch-like, round, mass-like, and stellate.[28] In our study, different cell types of human and mouse origins such as MCF7, MDA-MB-231, 3T3, A549, HEK293, A431, HepG2, and SiHa were cultured as 3-D spheroids using EW. The MCF7, 3T3, A431, and HepG2 spheroids appeared as highly organized masses, whereas MDA-MB-231, A549, HEK293, and SiHa spheroids appeared grape-bunch-like (Figures 10 and 11). The mass-like spheroids generally have cells exhibiting high cell−cell adhesion and disorganized nuclei filling the core. The grape bunch-like spheroids generally exhibit poor cell−cell adhesion and disorganized nuclei.[28,29] Despite the fact that spheroid formation is cell line specific, the original characteristics of cells such as proliferation, migration, and invasion are not affected by the spheroid morphology.[30,31] Importantly, the material and the physiomechanical properties of the culture system may exert a profound effect on spheroid morphology.[31] Evidently, the property of different internal morphologies with multiple scale structures, that is, nano to macro, and the apparent viscosity related to the ECM of soft tissues observed in EW may contribute to the control of spheroid organization by facilitating cell−cell and cell−ECM interactions. In addition, the stimuli received from cell−cell and cell−ECM interactions determine the polarity of cells in spheroids.[32−34] Measurement of the diameter of spheroids on days 3, 6, and 10 revealed that the spheroid size increased over the culture period. It was noted that the size of MCF7, MDA-MB-231, 3T3, and HEK293 spheroids reached almost 100 μm on day 10, whereas A549 and SiHa spheroids were very small on this day (Table 1).

2.7. Cell Proliferation. The results from the MTT assay indicate that EW facilitates proliferation of A549, MCF7, and HepG2 cells (Figure 12). In 3-D culture, the cell proliferation increased gradually even if the cells were cultured continuously for 10 days. The results show that cell growth in 3-D culture was slower than that in its monolayer counterpart. The results obtained from the quantification of genomic DNA are in good agreement with the MTT assay results (Figure 13). This is consistent with previous reports.[35,36] The results indicate that in 2-D culture all cells seeded on the plastic surface contact the medium, so they can proliferate and produce daughter cells till nutrients provided for and space allowed. The dead cells formed due to the crowding and the necrotic cells can be easily removed by changing the medium, and new daughter cells can replace that particular area, whereas in 3-D culture, the EW provides a larger area for cell proliferation all around, resulting in more counts of cells by improving and maintaining the proliferation rate. Also, the cells in the spheroids may pile up as layers one over the other to define an external proliferating zone and internal quiescent zone containing all states of cells such as viable, dead, and necrotic. Therefore, there is ability to maintain cell proliferation, but it is lesser with the 3-D format than 2-D. The mechanical stimuli of EW and the choice of cell lines can also affect the proliferation rate.[27,37−39] Also, the slow cell proliferation in 3-D culture is related to the differences in the gene expression pattern of growth promoting and restricting genes.[30,40,41]

2.8. Cytoskeletal Organization. The development of in vitro structural configuration resembling the native tissue

https://dx.doi.org/10.1021/acsomega.0c02508
ACS Omega XXXX, XXX, XXX−XXX

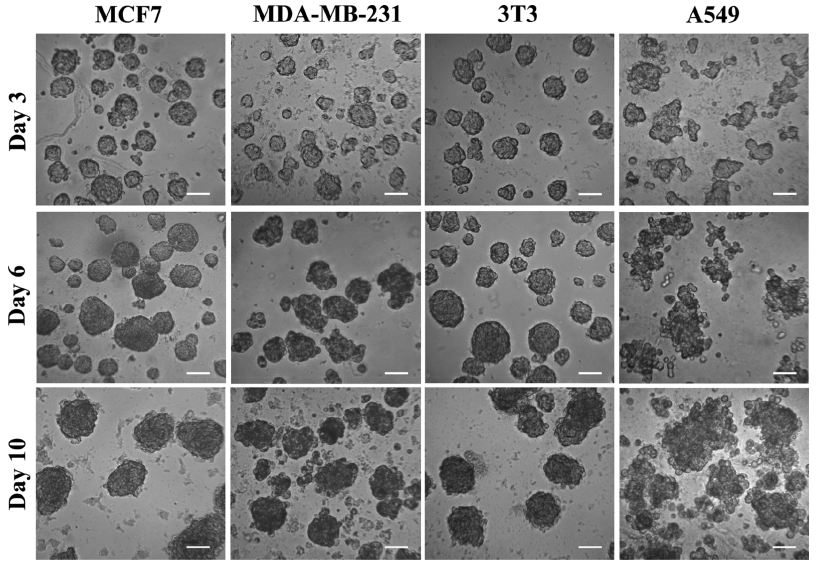

Figure 10. Light microscopic observation of spheroids of MCF7, MDA-MB-231, 3T3, and A549 cells on culture days 3, 6, and 10. Scale bar represents 50 μm.

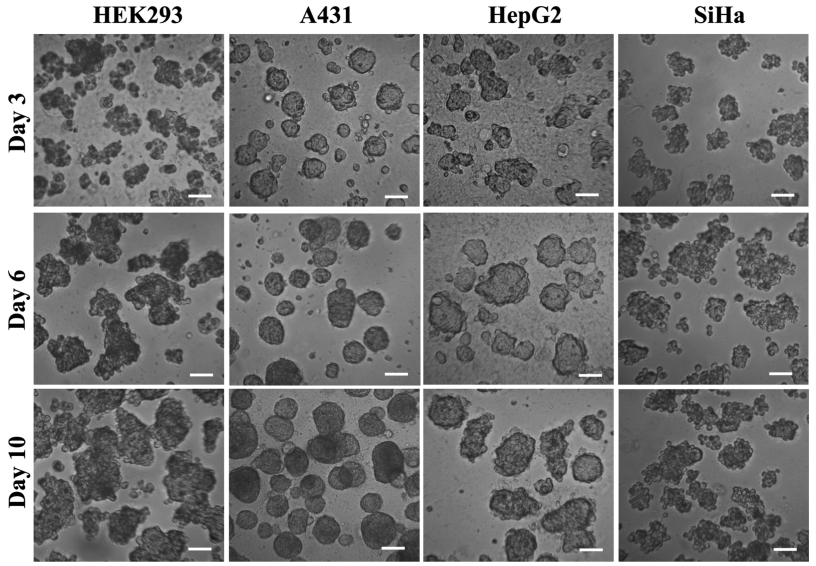

Figure 11. Light microscopic observation of spheroids of HEK293, A431, HepG2, and SiHa cells on culture days 3, 6, and 10. Scale bar represents 50 μm.

Table 1. Spheroid Diameter Measured from Microscopic Observations[a]

cell line	day 3	day 6	day 10
MCF7	51.99 ± 8.81	69.15 ± 7.64	97.47 ± 9.89
MDA-MB-231	52.10 ± 8.19	71.54 ± 5.99	92.11 ± 6.20
3T3	68.33 ± 1846	92.75 ± 19.38	103.54 ± 6.21
A549	59.04 ± 17.15	65.06 ± 5.67	69.40 ± 10.44
HEK293	42.18 ± 9.34	62.30 ± 10.21	94.94 ± 13.11
A431	67.00 ± 8.847	76.40 ± 6.74	80.43 ± 5.87
HepG2	54.22 ± 13.93	83.76 ± 5.64	85.26 ± 11.44
SiHa	57.93 ± 7.52	60.84 ± 7.02	73.35 ± 6.31

[a] μm, mean ± SE of 10 measurements each.

involves a series of cellular events that are closely related to dynamic cytoskeletal organization. Actin, the major component of the intercellular junctional cytoskeleton, contributes to cell−cell contact, cell maturity, tissue structure, and functionality.[42] In the present study the junctional filamentous actin (F-actin) filaments were intensely aggregated in the cortex and at the intercellular junctions throughout A549, MCF7, and HepG2 spheroids (Figure 14). The formation of junctional F-actin has been associated with the enhanced cellular adhesion and signal transduction indicating the preservation of the in vivo-like cytoarchitecture in the spheroids.[43] In contrast, the monolayer culture of all three cells shows stress fibers of F-actin in the cytoplasm at the middle section of monolayers. The results show prominent F-actin formation localized at the cell base in monolayer cells where cells attach to the surface of the tissue culture plates, instead of the cell−cell contact points. This subsequently decreases cell−cell adhesion and cell signaling, which consequently affects tissue-specific functions.[44]

2.9. Merits of EW over Hydrogels/Scaffolds for Culture of 3-D MTS. The EW as a medium to culture 3-D MTS has advantages as well as limitations. Unlike polysaccharides (e.g., alginate and chitosan), cellulose (e.g.,

https://dx.doi.org/10.1021/acsomega.0c02508
ACS Omega XXXX, XXX, XXX−XXX

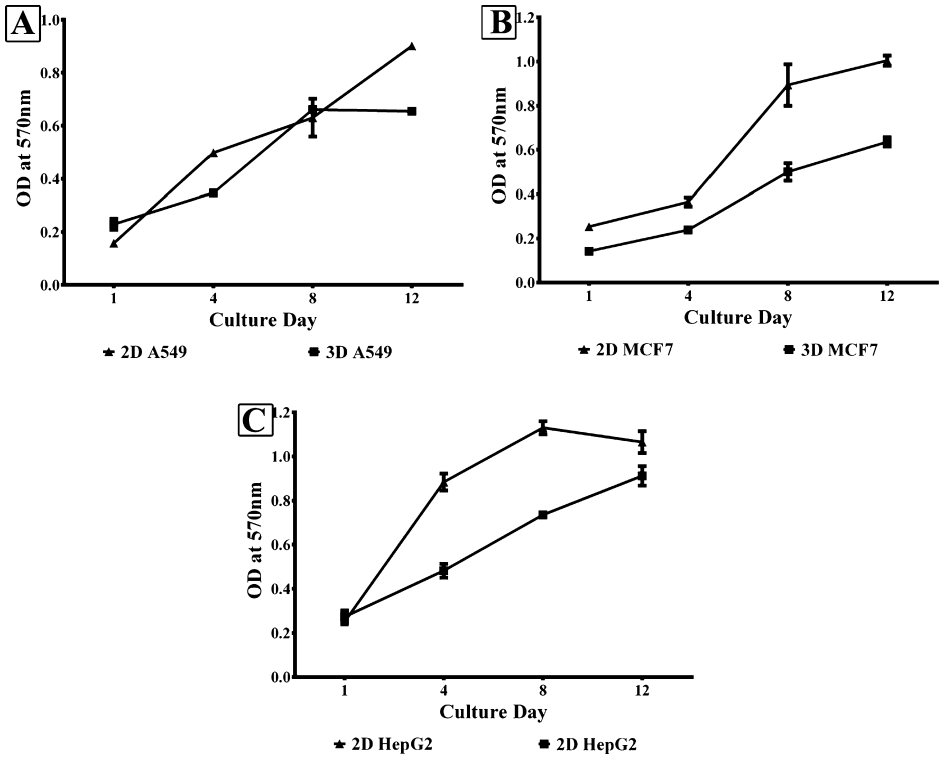

Figure 12. Comparison of proliferation efficiency between 2D culture and 3D spheroids of A549 (A) and MCF7 (B) and HepG2 (C) cells on days 1, 4, 8, and 12 adopting the MTT assay. Error bars represent mean ± SD (n = 3).

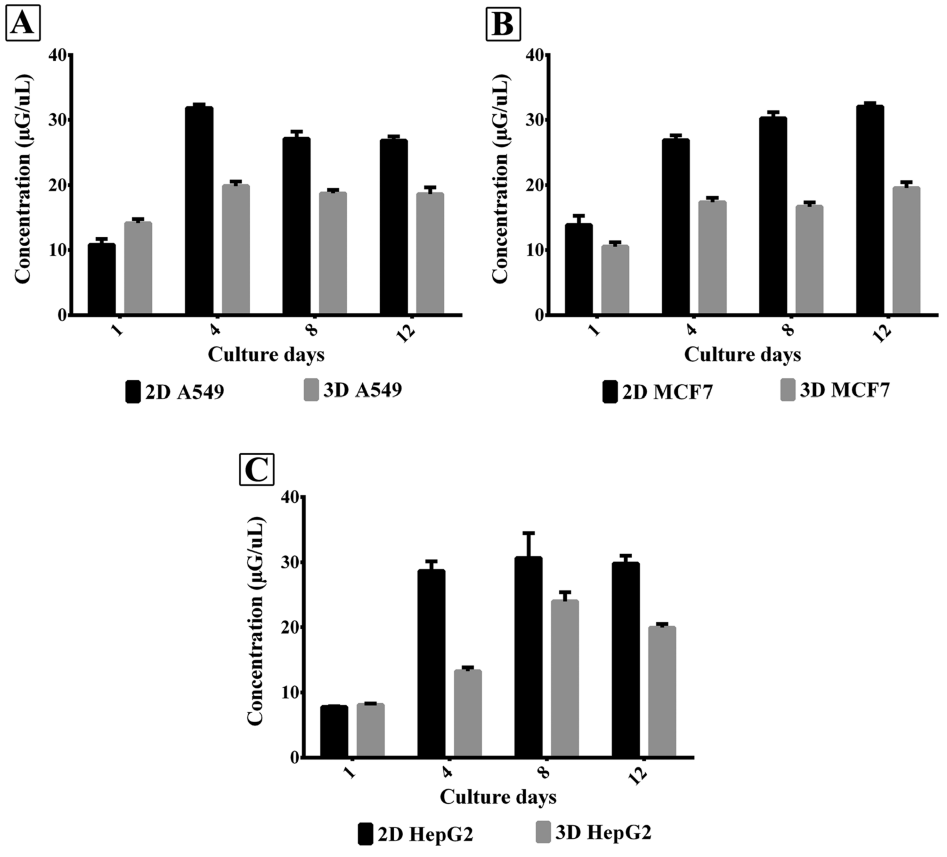

Figure 13. Difference in the rate of proliferation between 2D culture and 3D spheroids of A549 (A) and MCF7 (B) and HepG2 (C) cells on days 1, 4, 8, and 12 assessed by measuring the gDNA. Error bars represent mean ± SD (n = 3).

https://dx.doi.org/10.1021/acsomega.0c02508
ACS Omega XXXX, XXX, XXX−XXX

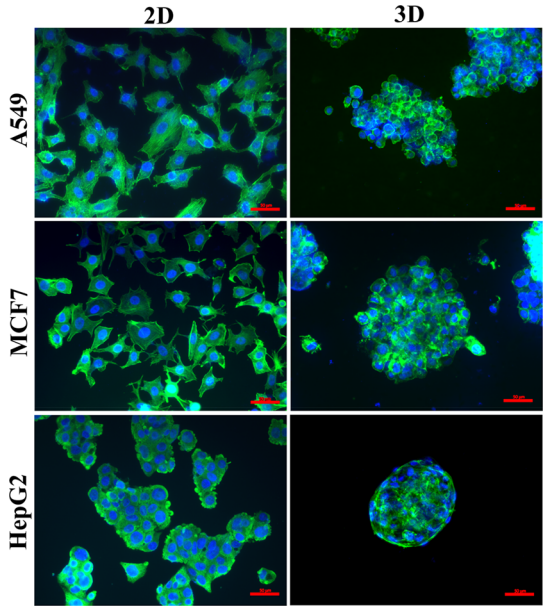

Figure 14. Immunostaining and comparison of junction marker F-actin between spheroid and monolayer cultures. Images from fluorescent staining show significant junctional F-actin (green color) at the points of cell−cell contact throughout 3-D cultured spheroids, whereas in cells cultured in monolayers, a large amount of F-actin cytoskeleton is distributed in the cell base area contacting the dish surface. Green and blue colors represent staining of F-actin and nuclear counterstain, respectively. Scale bar is 50 μm.

nanofibrillar cellulose), and synthetic materials (e.g., polyethylene glycol), EW is formed of proteins and so provides space, nutrients, and support to the cells in culture. Furthermore, the nano- to micron-level structures observed in EW may provide more binding moieties to the cells, which can potentially regulate cell functions. Also, the physiological properties of EW such as viscoelasticity can be modified simply by means of heat and cross-linking chemistry in such a way that EW can be used as a cost-effective bioink.[17,19,20] Nevertheless, as of now, it is difficult to find the specific endogenous factor(s) from among the mixture of EW proteins, which promote cell growth. Likewise, the impact of batch-to-batch variability on the reproducibility of the outcome requires further analysis.

3. CONCLUSIONS

This study deciphers hen's EW as a platform appropriate to grow 3-D MTSs. Investigation of the properties of microstructure, rheology, optical measurements, and biocompatibility are the important aspects to be concerned with in the context of a novel material for cell culture applications. The SEM analysis and particle size distribution measurement of EW showed different microstructures and confirm the nano- to micron-level particle size distribution. The observed rheological characteristics of EW provide information on viscoelasticity, and the results indicate that viscosity that exists in the EW is suitable to culture soft tissues. The reversible gelation property offers less resistance to the flow helping to reduce the shear stress. This fluid-like behavior was found to be suitable to handle the cells embedded in EW using microtips without affecting the viability of cells. As EW does not produce any absorbance peak between 400 and 700 nm, the observation of cells through a light microscope was not hindered. Also, the lack of autofluorescence in EW was of advantage to use it with a wide variety of fluorescent reagents. The protein-rich EW showed biocompatibility with the cells, and the specific volume of the EW practiced provides nutrient to the cells and promotes cell proliferation. 3-D MTS was successfully developed using different cell lines. The morphology, proliferation, cytoskeleton molecules such as F-actin involved in the important function of cell−cell, and cell−ECM interactions were compared between 3-D and 2-D cell cultures and the pre-eminence of the spheroid model over flat culture was evaluated in detail. Overall, this study indicates that the microstructures, advantageous rheological properties, and other important characteristics of the EW facilitate the formation of spheroids of different cell types. More importantly, this cost-affordable and easy-to-isolate EW, having bioactive substances that act as the in vivo-like ECM, is of advantage for the growth of cells as 3-D MTS without any additional ECM components.

4. MATERIALS

4.1. Cell Lines and Maintenance. Human breast cancer cells MCF7 and MDA-MB-231, human lung cancer cell A549, human embryonic kidney cell HEK293, human epidermoid carcinoma cell A431, human liver carcinoma cell HepG2, human cervical cancer cell SiHa, and mouse fibroblast cell 3T3 were obtained from National Center for Cell Science (NCCS), Pune, India. The cells were cultured in high-glucose DMEM and RPMI 1640 media (Sigma-Aldrich, USA), supplemented with 10% fetal bovine serum, and 2% penicillin, and streptomycin as antibiotics (Gibco, Thermo Scientific, USA). Cells were maintained in the exponential phase at 37 °C in a humidified atmosphere of 5% CO_2 in a CO_2 incubator (Thermo Scientific, USA).

4.2. Reagents and Plasticwares. Trypsin EDTA (0.25%) and 3-(4,5-dimethylthiazol-2-yl)-2,5-diphenyltetrazolium bromide (MTT) were supplied by HiMedia, India. The dyes Alexa Fluor 532 phalloidin, hoechst-33258, acridine orange, and rhodamine 123 were purchased from Invitrogen, Thermo Fisher, USA. The GenElute genomic DNA prep kit was supplied by Sigma-Aldrich, USA. All other chemicals and reagents used were of analytical grade, obtained from EMPLURA, Sigma-Aldrich, USA and HiMedia, India. Tissue culture plasticware products were obtained from HiMedia, India.

4.3. Egg White. Chicken (*Gallus gallus domesticus*; White Leghorn breed) eggs were purchased from a local vendor. The egg shell was punctured using an egg hole puncher and EW was collected in a sterile beaker. The EW was gently stirred and refrigerated at 8 °C.

5. METHODS

5.1. SEM Analysis. The morphological features of the EW were analyzed using a field emission scanning electron microscope. The lyophilized samples were sputter-coated with gold (Emitech, SC7620) for FESEM micrograph measurements (Carl Zeiss, Germany). Particle size, pore size, and their size distribution profiles were determined from at least 50 measurements on SEM images using image analysis software (ImageJ 1.50i).

5.2. DLS and Zeta Potential Measurements. The hydrodynamic size distribution in EW was analyzed in a Malvern zeta sizerNano ZS90 apparatus at 25 °C, illuminating

https://dx.doi.org/10.1021/acsomega.0c02508
ACS Omega XXXX, XXX, XXX−XXX

the sample by 633 nm radiation from a solid state He−Ne laser, and the scattered light was collected at an angle of 90°. All measurements were made in triplicate.

5.3. Rheological Measurements. The rheological properties of EW were measured at room temperature with a strain-controlled rheometer (Physica MCR 301, Anton Paar, Austria) equipped with a parallel-plate geometry. The diameter of the measuring plate was 12.5 mm. The steady-state viscosity of EW was measured against the shear stress range of 0.01−100 Pa. The viscoelastic properties of the EW were characterized using frequency sweep measurements from 0.1 to 100 rad/s at a constant strain of 30%.

5.4. Injectability of EW for Cell Culture. The injectability of EW to dispense the cells was measured according to Bhattacharya et al.[25] Cells were initially cultured routinely in T25/T75 flasks for 48 h prior to the injection. Cell culture in EW was initiated by mixing A549 cells with the EW at a density of 2.5×10^3 cells per 200 μL in a 96-well plate using a 1 mL syringe and needles of different gauge sizes (#20, 21, 23, 24, 25, and 26). After transfer, the cells were cultured for another 24 h, and thereafter, the viability was checked using the MTT assay (elaborate protocol is provided in Section 5.6).[45] The mean OD values from six replicate experiments were used to plot the graph.

5.5. Optical Properties. The optical property of EW was characterized to determine the transparency of EW in terms of observing cellular behavior in microscopic detection. The absorbance and fluorescence properties of EW were recorded according to Bhattacharya et al.[25] with a slight modification. UV−vis absorbance of EW was recorded in the range of 200−700 nm using a UV−vis spectrometer (Multiskan GO, Thermo Scientific, USA). The fluorescence spectra of EW after excitation at 350, 480, and 511 nm were measured using a spectrofluorimeter (Jasco, USA). The excitation wavelengths were most commonly used in biological imaging.[46,47] Hoechst 33258 (10 μg/mL), acridine orange (6 μg/mL), and rhodamine 123 (10 mM) were used as the reference for each excitation wavelength. Purified water was used as the negative control.

5.6. Biocompatibility Characterization. For the analysis of biocompatibility, EW was infused with different cell types such as A549, MCF7, HepG2, and HEK293. Different proportions of EW and growth media were mixed and added to wells of the 96 culture plate. The total volume in each well was set to be 200 μL and EW/culture media were prepared in five proportions, 0:200, 50:150, 100:100, 150:50, and 200:0 for groups 1, 2, 3, 4, and 5, respectively. After 48 h incubation at 37 °C with 5% CO_2, 20 μL of the MTT working solution (5 mg/mL in PBS) was transferred to wells of the 96 culture plate. After incubation for 4 h at 37 °C, the formazan crystals were dissolved in 100 μL of dimethyl sulfoxide (DMSO). The absorbance of the purple color was determined at 570 nm with a reference wavelength of 630 nm (iMark, Bio-Rad, USA). Data were collected for three replicates each and used to calculate the respective means. The average OD570 of untreated cells was set as 100%. Then, the percentage of viability in EW-exposed samples was measured by comparison of the average OD_{570} values of treated cells with the OD_{570} value of the untreated cells. The results of biocompatibility analysis are presented as means ± SD of three experimental replicates.

5.7. 3-D and 2-D Cultures. The EW was used to support the culture of different cell types in the 3-D spheroid culture format. The cells MCF7, MDA-MB-231, 3T3, A549, HEK293, A431, HepG2, and SiHa were cultured in 2-D and 3-D formats. In order to conduct 2-D cell culture, the cells maintained in the culture flasks were detached using trypsin. 5×10^4 cells were seeded in the wells of standard 24-well cell culture plates, which were already fed with the culture medium, and incubated at 37 °C and 5% CO_2. The medium was replaced every 2 days. The number of cells seeded in 2-D was maintained the same throughout the study.

The cells for 3-D culture were prepared as for standard monolayer cell culture. After trypsinization, 1×10^5 cells were mixed with EW to achieve typically 1000 cells/μL. The cell−EW mixture was added onto 24-well ultralow attachment plates. An equal volume of growth medium was added on top of the cell−EW mixture and cultured at 37 °C and 5% CO_2. The medium was replaced every 2 days without disturbing the cells.

5.8. Morphological Analysis of Spheroids. Formation of spheroids of MCF7, MDA-MB-231, 3T3, A549, HEK293, A431, HepG2, and SiHa cells was monitored using an inverted light microscope (Axiovert 40 CFL, Carl Zeiss, Germany) and images were obtained on days 3, 6, and 10. The profile shape of the spheroids was classified into four categories—round, mass, grape, and stellate according to Edmondson *et al.*[48] The diameters of spheroids from each well were measured using Carl Zeiss Zen 2012 software during the light microscopic observation. Diameters of more than 10 spheroids were used to calculate the average spheroid size in each group.

5.9. Analysis of Cell Proliferation. The proliferation efficiency of cells in spheroids and 2-D format was quantified using the MTT assay and determination of genomic DNA. At specific intervals (days 1, 4, 8, and 12), A549, MCF7, and HepG2 cells were cultured as spheroids as well as in the monolayer format, analyzed, and compared.

5.9.1. MTT Assay. The MTT assay was used to measure the proliferation efficiency of cells according to Mosmann.[45] The spheroids and 2-D cultures were subjected to a standard protocol reported by Balaji *et al.*[20] with slight modifications. With respect to spheroid culture, after the specific intervals (days 1, 4, 8, and 12), 50 μL of the working MTT solution from the stock (5 mg/mL) was added to the particular wells of a 24-well plate. After 3 h incubation in a 5% CO_2 incubator (95% humidity, 37 °C), the whole content, including the spheroids, was centrifuged at 1000 rpm (3−4 min). The formazan crystals in the cells were dissolved in 1 mL of DMSO; 200 μL of the solution was transferred to the 96-well plate to measure the absorbance.

Similarly, the cells in 2D culture were treated with 50 μL of the working MTT solution. After 3 h incubation, the formazan crystals were dissolved by adding 1 mL of DMSO; 200 μL of the solution was transferred to the 96-well plate to measure the absorbance at 570 nm with 630 nm as reference in a plate reader (iMark, Bio-Rad, USA).

5.9.2. DNA Quantification Assay. Proliferation efficiency of the cells cultured in 2-D and 3-D formats was furthermore analyzed by measuring the gDNA content using the GenElute mammalian genomic DNA prep kit. After the specific incubation period (1, 4, 8, and 12 days), the cells were collected, lysed, pooled, and subjected to processing as prescribed by the manufacturer. The concentration of the extracted gDNA was measured using a UV−vis spectrometer (Multiskan GO, Thermo Scientific, USA).

https://dx.doi.org/10.1021/acsomega.0c02508
ACS Omega XXXX, XXX, XXX−XXX

5.10. F-Actin Staining. The morphology and cytoskeletal organization of the spheroids and the cells cultured as 2-D were analyzed by capturing the F-actin orientation by phalloidin staining. Briefly, the cultured spheroids or cells were fixed in 4% formalin for 15 min at 4 °C. Following washing with PBS, the cells were permeabilized with 0.1% Triton X-100 and incubated overnight with Alexa Fluor 488-labeled phalloidin to stain the filamentous actin. The spheroids were then counterstained with Hoechst 33258 and visualized using a fluorescent microscope (Axio Observer 7, Carl Zeiss, Germany). The fluorescent emission was captured at 525 and 461 nm for phalloidin and hoechst, respectively.

5.11. Statistical Analysis. The data were subjected to statistical analysis using PRISM version 6.0 software (GraphPad Software, La Jolla, CA, USA). Data obtained from the injectability analysis were subjected to one-way ANOVA, and the results are presented as means ± SD of six experimental replicates. Data obtained from the MTT assay and biocompatibility characterization were subjected to two-way ANOVA, and the results are presented as means ± SD of three experimental replicates. The data from SEM analysis and diameter measurement of spheroids were analyzed using Microsoft Office Excel 2007, where $p < 0.05$ was considered statistically significant.

AUTHOR INFORMATION

Corresponding Author

Mohammad Abdulkader Akbarsha − *National College (Autonomous), Tiruchirappalli 620001, India; Mahatma Gandhi-Doerenkamp Centre for Alternatives, Bharathidasan University, Tiruchirappalli 620 024, India;* orcid.org/0000-0002-4313-9606; Phone: +919790995854; Email: akbarbdu@gmail.com

Authors

Perumalsamy Balaji − *Department of Biomedical Science and National Centre for Alternatives to Animal Experiments, Bharathidasan University, Tiruchirapalli 620024, India*

Anbazhagan Murugadas − *Department of Pediatrics, School of Medicine, Emory University, Atlanta, Georgia 30322, United States; National Centre for Alternatives to Animal Experiments, Bharathidasan University, Tiruchirappalli 620 024, India*

Arunachalam Ramkumar − *Department of Environmental Biotechnology and National Centre for Alternatives to Animal Experiments, Bharathidasan University, Tiruchirapalli 620024, India*

Ramasamy Thirumurugan − *Department of Animal Science and National Centre for Alternatives to Animal Experiments, Bharathidasan University, Tiruchirapalli 620024, India*

Sellathamby Shanmugaapriya − *Department of Biomedical Science, Bharathidasan University, Tiruchirapalli 620024, India*

Complete contact information is available at: https://pubs.acs.org/10.1021/acsomega.0c02508

Author Contributions

The manuscript was written through contributions of all authors. All authors have given approval to the final version of the manuscript.

Notes

The authors declare no competing financial interest.

ACKNOWLEDGMENTS

This work was carried out at Mahatma Gandhi-Doerenkamp Center for Alternatives to Use of Animals in Life Science Education, Bharathidasan University, Tiruchirappalli—620024, established by Doerenkamp-Zbinden Foundation, Switzerland. This work was partially supported by National Center for Alternatives to Animal Experiments (NCAAE), funded by UGC, Government of India [F.no. 2-1/2013(NS/PE)].

ABBREVIATIONS

DMSO, dimethyl sulfoxide; MTT, 3-4,5-dimethylthiazole-2-yl,2,5-diphenyl tetrazoliumbromide; G', storage module; G'', loss module; F-actin, filamentous actin

REFERENCES

(1) Lv, D.; Hu, Z.; Lu, L.; Lu, H.; Xu, X. Three-dimensional cell culture: A powerful tool in tumor research and drug discovery. *Oncol. Lett.* **2017**, *14*, 6999−7010.

(2) Kelm, J. M.; Timmins, N. E.; Brown, C. J.; Fussenegger, M.; Nielsen, L. K. Method for generation of homogeneous multicellular tumor spheroids applicable to a wide variety of cell types. *Biotechnol. Bioeng.* **2003**, *83*, 173−180.

(3) Bazzoun, D.; Lelièvre, S.; Talhouk, R. Polarity proteins as regulators of cell junction complexes: implications for breast cancer. *Pharmacol. Ther.* **2013**, *138*, 418−427.

(4) Delarue, M.; Montel, F.; Vignjevic, D.; Prost, J.; Joanny, J.-F.; Cappello, G. Compressive stress inhibits proliferation in tumor spheroids through a volume limitation. *Biophys. J.* **2014**, *107*, 1821−1828.

(5) Pampaloni, F.; Reynaud, E. G.; Stelzer, E. H. K. The third dimension bridges the gap between cell culture and live tissue. *Nat. Rev. Mol. Cell Biol.* **2007**, *8*, 839−845.

(6) Ma, H.-l.; Jiang, Q.; Han, S.; Wu, Y.; Tomshine, J. C.; Wang, D.; Gan, Y.; Zou, G.; Liang, X.-J. Multicellular tumor spheroids as an in vivo−like tumor model for three-dimensional imaging of chemotherapeutic and nano material cellular penetration. *Mol. Imag.* **2012**, *11*, 487−498.

(7) Vidi, P.-A.; Bissell, M. J.; Lelièvre, S. A. Three-dimensional culture of human breast epithelial cells: the how and the why. In *Epithelial Cell Culture Protocols*; Randell, S., Fulcher, M., Eds.; Humana Press: Totowa, NJ, 2012; pp 193−219.

(8) Infanger, D. W.; Cho, Y.; Lopez, B. S.; Mohanan, S.; Liu, S. C.; Gursel, D.; Boockvar, J. A.; Fischbach, C. Glioblastoma stem cells are regulated by interleukin-8 signaling in a tumoral perivascular niche. *Cancer Res.* **2013**, *73*, 7079−7089.

(9) Durand, R. E.; Raleigh, J. A. Identification of nonproliferating but viable hypoxic tumor cells in vivo. *Cancer Res.* **1998**, *58*, 3547−3550.

(10) Lin, R.-Z.; Chang, H.-Y. Recent advances in three-dimensional multicellular spheroid culture for biomedical research. *Biotechnol. J.* **2008**, *3*, 1172−1184.

(11) Baker, B. M.; Chen, C. S. Deconstructing the third dimension: how 3D culture microenvironments alter cellular cues. *J. Cell Sci.* **2012**, *125*, 3015−3024.

(12) Drury, J. L.; Mooney, D. J. Hydrogels for tissue engineering: scaffold design variables and applications. *Biomaterials* **2003**, *24*, 4337−4351.

(13) Stevens, L. Egg white proteins. *Comp. Biochem. Physiol., Part B: Biochem. Mol. Biol.* **1991**, *100*, 1−9.

(14) Mine, Y. Recent advances in the understanding of egg white protein functionality. *Trends Food Sci. Technol.* **1995**, *6*, 225−232.

(15) Ruan, G.-P.; Wang, J.-X.; Pang, R.-Q.; Yao, X.; Cai, X.-M.; Wang, Q.; Ma, L.-H.; Zhu, X.-Q.; Pan, X.-H. Treatment with chicken-egg-white or whole-egg extracts maintains and enhances the survival and differentiation of spleen cells. *Cytotechnology* **2012**, *64*, 541−551.

(16) Mizunoya, W.; Tashima, A.; Sato, Y.; Tatsumi, R.; Ikeuchi, Y. The growth-promoting activity of egg white proteins in the C2C12 myoblast cell line. *Anim. Sci. J.* **2015**, *86*, 194−199.
(17) Kaipparettu, B. A.; Kuiatse, I.; Tak-Yee Chan, B.; Benny Kaipparettu, M.; Lee, A. V.; Oesterreich, S. Novel egg white-based 3-D cell culture system. *Biotechniques* **2008**, *45*, 165−171.
(18) Mohan, N.; Nair, P. D.; Tabata, Y. A 3D biodegradable protein based matrix for cartilage tissue engineering and stem cell differentiation to cartilage. *J. Mater. Sci.: Mater. Med.* **2009**, *20*, 49−60.
(19) Jalili-Firoozinezhad, S.; Rajabi-Zeleti, S.; Mohammadi, P.; Gaudiello, E.; Bonakdar, S.; Solati-Hashjin, M.; Marsano, A.; Aghdami, N.; Scherberich, A.; Baharvand, H.; Martin, I. Facile fabrication of egg white macroporous sponges for tissue regeneration. *Adv. Healthcare Mater.* **2015**, *4*, 2281−2290.
(20) Balaji, P.; Murugadas, A.; Shanmugaapriya, S.; Abdulkader Akbarsha, M. Fabrication and characterization of egg white cryogel scaffold for three-dimensional (3D) cell culture. *Biocatal. Agric. Biotechnol.* **2019**, *17*, 441−446.
(21) Putzeys, P.; Brosteaux, J. The scattering of light in protein solutions. *Trans. Faraday Soc.* **1935**, *31*, 1314−1325.
(22) Heller, W.; Klevens, H. Molecular weights of proteins as determined by light scattering. *Physical Review*; American Physical Society, One Physics Ellipse: College Park, Maryland USA, 1945; p 61.
(23) Abdou, A.; Kim, M.; Sato, K. Functional proteins and peptides of hen's egg origin. *Bioactive Food Peptides in Health and Disease*; IntechOpen: London, U.K., 2013; pp 115−116.
(24) Miron-Mendoza, M.; Seemann, J.; Grinnell, F. The differential regulation of cell motile activity through matrix stiffness and porosity in three dimensional collagen matrices. *Biomaterials* **2010**, *31*, 6425−6435.
(25) Bhattacharya, M.; Malinen, M. M.; Lauren, P.; Lou, Y.-R.; Kuisma, S. W.; Kanninen, L.; Lille, M.; Corlu, A.; GuGuen-Guillouzo, C.; Ikkala, O.; Laukkanen, A.; Urtti, A.; Yliperttula, M. Nanofibrillar cellulose hydrogel promotes three-dimensional liver cell culture. *J. Controlled Release* **2012**, *164*, 291−298.
(26) Friedrich, J.; Eder, W.; Castaneda, J.; Doss, M.; Huber, E.; Ebner, R.; Kunz-Schughart, L. A. A reliable tool to determine cell viability in complex 3-d culture: the acid phosphatase assay. *J. Biomol. Screening* **2007**, *12*, 925−937.
(27) Weiss, M. S.; Bernabé, B. P.; Shikanov, A.; Bluver, D. A.; Mui, M. D.; Shin, S.; Broadbelt, L. J.; Shea, L. D. The impact of adhesion peptides within hydrogels on the phenotype and signaling of normal and cancerous mammary epithelial cells. *Biomaterials* **2012**, *33*, 3548−3559.
(28) Kenny, P. A.; Lee, G. Y.; Myers, C. A.; Neve, R. M.; Semeiks, J. R.; Spellman, P. T.; Lorenz, K.; Lee, E. H.; Barcellos-Hoff, M. H.; Petersen, O. W.; Gray, J. W.; Bissell, M. J. The morphologies of breast cancer cell lines in three-dimensional assays correlate with their profiles of gene expression. *Mol. Oncol.* **2007**, *1*, 84−96.
(29) Härmä, V.; Virtanen, J.; Mäkelä, R.; Happonen, A.; Mpindi, J.-P.; Knuuttila, M.; Kohonen, P.; Lötjönen, J.; Kallioniemi, O.; Nees, M. A comprehensive panel of three-dimensional models for studies of prostate cancer growth, invasion and drug responses. *PLoS One* **2010**, *5*, No. e10431.
(30) Luca, A. C.; Mersch, S.; Deenen, R.; Schmidt, S.; Messner, I.; Schäfer, K.-L.; Baldus, S. E.; Huckenbeck, W.; Piekorz, R. P.; Knoefel, W. T.; Krieg, A.; Stoecklein, N. H. Impact of the 3D microenvironment on phenotype, gene expression, and EGFR inhibition of colorectal cancer cell lines. *PLoS One* **2013**, *8*, No. e59689.
(31) Hongisto, V.; Jernström, S.; Fey, V.; Mpindi, J.-P.; Kleivi Sahlberg, K.; Kallioniemi, O.; Perälä, M. High-throughput 3D screening reveals differences in drug sensitivities between culture models of JIMT1 breast cancer cells. *PLoS One* **2013**, *8*, No. e77232.
(32) Petersen, O. W.; Ronnov-Jessen, L.; Howlett, A. R.; Bissell, M. J. Interaction with basement membrane serves to rapidly distinguish growth and differentiation pattern of normal and malignant human breast epithelial cells. *Proc. Natl. Acad. Sci. U.S.A.* **1992**, *89*, 9064−9068.
(33) Griffith, L. G.; Swartz, M. A. Capturing complex 3D tissue physiology in vitro. *Nat. Rev. Mol. Cell Biol.* **2006**, *7*, 211−224.
(34) Cawkill, D.; Eaglestone, S. S. Evolution of cell-based reagent provision. *Drug Discovery Today* **2007**, *12*, 820−825.
(35) Khaitan, D.; Chandna, S.; Arya, M.; Dwarakanath, B. Establishment and characterization of multicellular spheroids from a human glioma cell line; Implications for tumor therapy. *J. Transl. Med.* **2006**, *4*, 12.
(36) Gurski, L. A.; Jha, A. K.; Zhang, C.; Jia, X.; Farach-Carson, M. C. Hyaluronic acid-based hydrogels as 3D matrices for in vitro evaluation of chemotherapeutic drugs using poorly adherent prostate cancer cells. *Biomaterials* **2009**, *30*, 6076−6085.
(37) Semino, C. E.; Merok, J. R.; Crane, G. G.; Panagiotakos, G.; Zhang, S. Functional differentiation of hepatocyte-like spheroid structures from putative liver progenitor cells in three-dimensional peptide scaffolds. *Differentiation* **2003**, *71*, 262−270.
(38) Park, J. S.; Woo, D. G.; Sun, B. K.; Chung, H.-M.; Im, S. J.; Choi, Y. M.; Park, K.; Huh, K. M.; Park, K.-H. In vitro and in vivo test of PEG/PCL-based hydrogel scaffold for cell delivery application. *J. Controlled Release* **2007**, *124*, 51−59.
(39) Wang, X.; Sun, L.; Maffini, M. V.; Soto, A.; Sonnenschein, C.; Kaplan, D. L. A complex 3D human tissue culture system based on mammary stromal cells and silk scaffolds for modeling breast morphogenesis and function. *Biomaterials* **2010**, *31*, 3920−3929.
(40) Birgersdotter, A.; Sandberg, R.; Ernberg, I. Gene expression perturbation in vitro–a growing case for three-dimensional (3D) culture systems. *Semin. Cancer Biol.* **2005**, *15*, 405−412.
(41) Gurski, L. A.; Petrelli, N. J.; Jia, X.; Farach-Carson, M. C. 3D Matrices for Anti-Cancer Drug Testing and Development. *Oncol. Issues* **2017**, *25*, 20−25.
(42) Chu, Y.-S.; Thomas, W. A.; Eder, O.; Pincet, F.; Perez, E.; Thiery, J. P.; Dufour, S. Force measurements in E-cadherin-mediated cell doublets reveal rapid adhesion strengthened by actin cytoskeleton remodeling through Rac and Cdc42. *J. Cell Biol.* **2004**, *167*, 1183−1194.
(43) Zhang, J.; Betson, M.; Erasmus, J.; Zeikos, K.; Bailly, M.; Cramer, L. P.; Braga, V. M. Actin at cell-cell junctions is composed of two dynamic and functional populations. *J. Cell Sci.* **2005**, *118*, 5549−5562.
(44) Abu-Absi, S. F.; Friend, J. R.; Hansen, L. K.; Hu, W.-S. Structural polarity and functional bile canaliculi in rat hepatocyte spheroids. *Exp. Cell Res.* **2002**, *274*, 56−67.
(45) Mosmann, T. Rapid colorimetric assay for cellular growth and survival: application to proliferation and cytotoxicity assays. *J. Immunol. Methods* **1983**, *65*, 55−63.
(46) Tsien, R. Y.; Waggoner, A. Fluorophores for confocal microscopy. In *Handbook of biological confocal microscopy*; Pawley, J., Ed.; Springer: Boston, MA, 1995; pp 338−352.
(47) Liu, J.; Liu, C.; He, W. Fluorophores and their applications as molecular probes in living cells. *Curr. Org. Chem.* **2013**, *17*, 564−579.
(48) Edmondson, R.; Broglie, J. J.; Adcock, A. F.; Yang, L. Three-dimensional cell culture systems and their applications in drug discovery and cell-based biosensors. *Assay Drug Dev. Technol.* **2014**, *12*, 207−218.

https://dx.doi.org/10.1021/acsomega.0c02508
ACS Omega XXXX, XXX, XXX−XXX